Mausam, (1983), **34**, 4, 359-366

551.509.313 : 551.515.1 (541.5) "1982"

Numerical simulation of the surge generated by the June 1982 Orissa cyclone

P. K. DAS*
India Meteorological Department, New Delhi
and
S. K. DUBE, U. C. MOHANTY, P. C. SINHA & A. D. RAO
Centre for Atmospheric Sciences, Indian Institute of Technology, New Delhi

(Received 24 January 1983)

सार — उड़ीसा में आए जून 1982 के चक्रवात से उत्पन्न महोर्मि के आकलन में तटीय प्रदेश संख्यात्मक निदर्श का उपयोग किया गया है। इस निदर्श में विश्लेषण के लिए भारत के पूर्वी तट के साथ का 6° उ० अ० से लगभग 22° उ० अ० तक का क्षेत्र और खुले समुद्र में तट से औसतन 300 कि० मी० की सीमा का उपयोग किया गया है। इस निदर्श में तट रेखाओं को प्रदर्शित करने के लिए वक्ररेखी परिसीमा उपचार तथा तटीय सीमा के निकट असम अपतट ग्रिड स्पेसिंग का उपयोग किया गया है। इससे उड़ीसा तट के समीप विभेदन में वृद्धि हो जाती है।

उड़ीसा चक्रवात का प्रतिनिधित्व करने वाले प्रणोदन पवन प्रतिबल बंटन का उपयोग करके हमने निदर्श से प्रायुक्त महोर्मियों की पारादीप के उत्तर में उड़ीसा तट के एक भाग पर प्रेक्षित समुद्री सतह उत्थापनों से तुलना की है। समुद्र माध्य स्तर के ऊपर प्रायुक्त शिखर महोर्मि के उत्थापन और पारादीप पोर्ट एवं धामरा बन्दरगाह पर प्रेक्षित मानों में काफी समानता है।

ABSTRACT. A coastal zone numerical model has been used to estimate the surge generated by the June 1982 Orissa cyclone. In this model the analysis area extends from 6 N to about 22 N along the east coast of India and there is an open-sea boundary situated, on average, about 300 km from the coast. The model utilises a curvilinear boundary treatment to represent the coastlines and uses a non-uniform off-shore grid-spacing adjacent to the coastal boundaries. This allows an increased resolution near the Orissa coast.

Using a forcing wind-stress distribution representative of the Orissa cyclone, we compare the model predicted surges with the observed sea-surface elevations along part of the Orissa coast north of Paradip. The predicted peak surge elevation above mean sea level compares well with the observed values at the Paradip port and Dhamra harbour.

1. Introduction

A servere cyclonic storm with wind speed of about 100 to 110 kt struck the north Orissa coast on the night of 3 June 1982 at 2130 IST. Under its influence high surges were generated and the coastal stretch extending from Paradip to Balasore was affected due to saline water inundation. All along this coastal stretch heavy damage was caused to the paddy fields, roads, buildings, irrigation embankments, as a result of high tides.

The cyclonic storm which formed over the east central Bay of Bengal on 1 June 1982 and was expected to cause a gale wind with speed of 40 to 45 kt suddenly intensified into a severe cyclonic storm with wind speed of 85 to 110 kt in the afternoon of 3 June. The track of the cyclone, which has been constructed on the basis of synoptic and radar fixes of the storm centre, is shown in Fig. 1.

In the present paper an attempt has been made to simulate numerically the surge generated by this cyclonic storm. A number of models have been developed for simulating the surges in the Bay of Bengal by serveral workers (Das 1972; Das *et al.* 1974; Das 1981; Johns and Ali 1980; Johns 1981; Johns *et al.* 1981, 1982, 1983a, 1983b, etc). In our simulation experiment we use a coastal zone model, the dynamical formulation of which has been discussed by Johns *et al.* (1983 a). The analysis area of the model is shown in Fig. 2. On average, the width of the coastal zone is about 300 km and the coastline is represented by a realistic curvilinear boundary treatment analogous to that reported by Johns *et al.* (1981). The model uses a non-uniform off-shore grid-spacing adjacent to coastal boundary which permits an increased resolution near the Orissa coast.

Numerical experiments performed with this model lead to a surge response along the north Orissa coast which is in good agreement with the observed values.

2. Basic dynamical formulation

The sphericity of the earth's surface is neglected and we use a system of rectangular cartesian coordinates in which the origin, O, is within the equilibrium level of the sea-surface. Ox points towards the east, Oy points towards the north and Oz is directed vertically upwards.

*Present affiliation : Department of Meteorology, University of Nairobi, Kenya

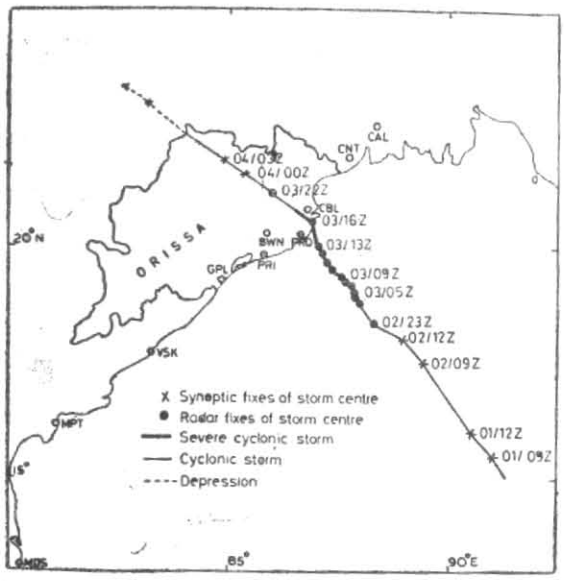

Fig. 1. Track of Orissa cyclone : 1-4 June 1982

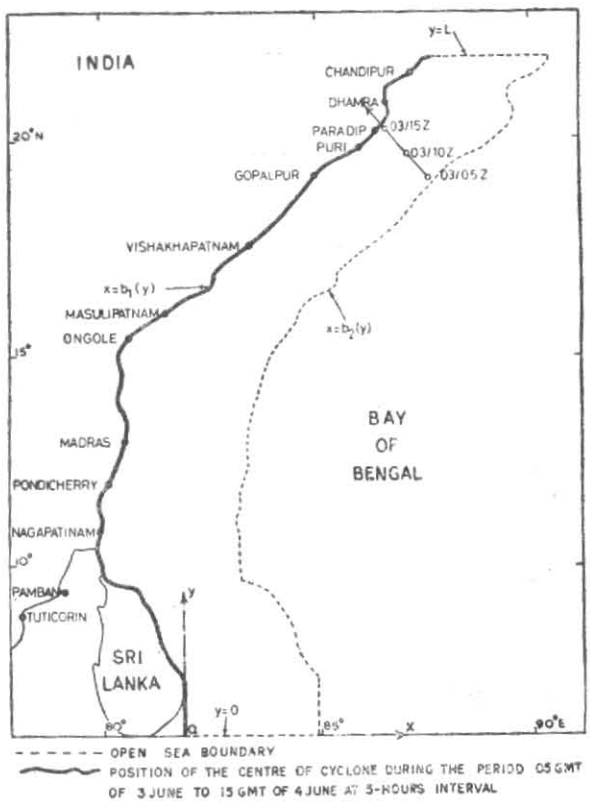

Fig. 2. Analysis area

The displaced position of the sea-surface is given by $z = \zeta(x, y, t)$ and the position of the sea-floor by $z = -h(x, y)$. A western coastal boundary (the east coast of India) is situated at $x = b_1(y)$ and an eastern open-sea boundary is at $x = b_2(y)$. Southern and northern open-sea boundaries are at $y = 0$ and $y = L$ respectively. This configuration is shown in Fig. 2.

The basic hydrodynamic equations of continuity and momentum for the dynamical processes in the sea, may then be given by:

$$\frac{\partial \zeta}{\partial t} + \frac{\partial}{\partial x}\left[(\zeta + h)\, u\right] + \frac{\partial}{\partial y}\left[(\zeta + h)\, v\right] = 0 \quad (1)$$

$$\frac{\partial u}{\partial t} + u\frac{\partial u}{\partial x} + v\frac{\partial u}{\partial y} - fv = -g\frac{\partial \zeta}{\partial x} + \frac{(\tau_x^{\zeta} - \tau_x^{-h})}{(\zeta + h)\,\rho} \quad (2)$$

$$\frac{\partial v}{\partial t} + u\frac{\partial v}{\partial x} + v\frac{\partial v}{\partial y} + fu = -g\frac{\partial \zeta}{\partial y} + \frac{(\tau_y^{\zeta} - \tau_y^{-h})}{(\zeta + h)\,\rho} \quad (3)$$

where,

f : coriolis parameter,

g : acceleration due to gravity,

t : time,

u, v : depth averaged currents of water towards the east and north respectively,

ρ : density of the sea-water,

$(\tau_x^{\zeta}, \tau_y^{\zeta})$: x and y components of wind stress and

$(\tau_x^{-h}, \tau_y^{-h})$: x and y components of bottom stress.

In writing the Eqns. (2) and (3), the pressure is taken as hydrostatic and the effect of astronomical tide generating forces and barometric forcing are omitted. The applied surface wind stress and the bottom stress are parameterised by a conventional quadratic law :

$$\tau_x^{\zeta} = C_0\, u_a\, (u_a^2 + v_a^2)^{\frac{1}{2}} \quad (4)$$

$$\tau_y^{\zeta} = C_0\, v_a\, (u_a^2 + v_a^2)^{\frac{1}{2}} \quad (5)$$

and $$\tau_x^{-h} = C_D\, u\, (u^2 + v^2)^{\frac{1}{2}} \quad (6)$$

$$\tau_y^{-h} = C_D\, v\, (u^2 + v^2)^{\frac{1}{2}} \quad (7)$$

where,

C_0 : uniform surface friction coefficient, which is taken as 2.8×10^{-3},

C_D : bottom friction coefficient, which is taken as 2.6×10^{-3} and

u_a, v_a : components of the wind towards the east and north respectively.

Following Johns *et al.* (1981, 1982, 1983 a), the lateral boundary conditions for the present model may be written as :

$$u - v\,\frac{\partial b_1}{\partial y} = 0 \quad \text{at } x = b_1(y) \tag{8}$$

$$u - v\,\frac{\partial b_2}{\partial y} - (g/h)^{\frac{1}{2}}\zeta = 0 \text{ at } x = b_2(y) \tag{9}$$

$$v + (g/h)^{\frac{1}{2}}\zeta = 0 \quad \text{at } y = 0 \tag{10}$$

$$v - (g/h)^{\frac{1}{2}}\zeta = 0 \quad \text{at } y = L \tag{11}$$

3. Coordinate transformation

In order to facilitate the numerical treatment of an irregular boundary configuration, we introduce a coodinate transformation (Johns *et al.* 1981), which is based upon a new set of independent variables, ξ, y and t where,

$$\xi = \frac{x - b_1(y)}{b(y)} \tag{12}$$

$$b(y) = b_2(y) - b_1(y) \tag{13}$$

Eqns. (1), (2) and (3) may then be transformed into

$$\frac{\partial}{\partial t}\left[\, b(y)\,\zeta \,\right] + \frac{\partial}{\partial \xi}\left[\, b(\zeta + h)\,U \,\right] + \frac{\partial \tilde{v}}{\partial y} = 0 \tag{14}$$

$$\frac{\partial \tilde{u}}{\partial t} + \frac{\partial}{\partial \xi}(U\,\tilde{u}) + \frac{\partial}{\partial y}(v\,\tilde{u}) - f\,\tilde{v} = -g(\zeta + h)\,\frac{\partial \zeta}{\partial \xi} + \frac{b\tau_x^{\zeta}}{\rho} - \frac{C_D\,\tilde{u}}{(\zeta + h)}\,(u^2 + v^2)^{\frac{1}{2}} \tag{15}$$

and

$$\frac{\partial \tilde{v}}{\partial t} + \frac{\partial}{\partial \xi}(U\,\tilde{v}) + \frac{\partial}{\partial y}(v\,\tilde{v}) + f\,\tilde{u} = -g(\zeta + h) \times \left[\, b\,\frac{\partial \zeta}{\partial y} - \left\{\frac{\partial b_1}{\partial y} + \xi\,\frac{\partial b}{\partial y}\right\}\frac{\partial \zeta}{\partial \xi}\,\right] + \frac{b\,\tau_y^{\zeta}}{\rho} - \frac{C_D\,\tilde{v}}{(\zeta + h)}\,(u^2 + v^2)^{\frac{1}{2}} \tag{16}$$

where,

$$b\,U = u - \left\{\frac{\partial b_1}{\partial y} + \xi\,\frac{\partial b}{\partial y}\right\}v \tag{17}$$

$$\left.\begin{aligned}\tilde{u} &= b(\zeta + h)\,u\\ \tilde{v} &= b(\zeta + h)\,v\end{aligned}\right\} \tag{18}$$

The lateral boundary conditions (8) and (9) become

$$U = 0 \quad \text{at } \xi = 0 \tag{19}$$

$$b(y)\,U - (g/h)^{\frac{1}{2}}\,\zeta = 0 \text{ at } \xi = 1 \tag{20}$$

Since the coastal surge elevations are effectively dependent upon the near-coastal bathymetry, a desirable feature of storm surge simulation schemes is the ability to incorporate increased resolution adjacent to the coastline. This is achieved by introducing a log-linear transformation (Johns *et al.* 1983 a) in which

$$\eta = \xi + \epsilon \ln\{(\xi + \xi_0)/\xi_0\} \tag{21}$$

where ϵ and ξ_0 are disposable parameters.

If we select $\epsilon = 0.04$ and $\xi_0 = 0.001$, it may be seen that the transformation (21) leads to a substantial grid refinement adjacent to coastal boundaries in which the first point off-shore of Paradip is about 7 km.

Taking η, y and t as new independent coordinates equations (14)-(16) then lead to

$$\frac{\partial}{\partial t}(b\,\zeta) + \frac{1}{F(\eta)}\,\frac{\partial}{\partial \eta}[b(\zeta + h)\,U] + \frac{\partial \tilde{v}}{\partial y} = 0 \tag{22}$$

$$\frac{\partial \tilde{u}}{\partial t} + \frac{1}{F(\eta)}\,\frac{\partial}{\partial \eta}(U\,\tilde{u}) + \frac{\partial}{\partial y}(v\,\tilde{u}) - f\,\tilde{v} = -\frac{g(\zeta + h)}{F(\eta)}\,\frac{\partial \zeta}{\partial \eta} + \frac{b\,\tau_x^{\zeta}}{\rho} - \frac{C_D\,\tilde{u}}{(\zeta + h)}\,(u^2 + v^2)^{\frac{1}{2}} \tag{23}$$

and

$$\frac{\partial \tilde{v}}{\partial t} + \frac{1}{F(\eta)}\,\frac{\partial}{\partial \eta}(U\,\tilde{v}) + \frac{\partial}{\partial y}(v\,\tilde{v}) + f\,\tilde{u} = -g(\zeta + h)\left[\, b\,\frac{\partial \zeta}{\partial y} - \left\{\frac{\partial b_1}{\partial y} + \xi\,\frac{\partial b}{\partial y}\right\} \times \frac{1}{F(\eta)}\,\frac{\partial \zeta}{\partial \eta}\,\right] + \frac{b\,\tau_y^{\zeta}}{\rho} - \frac{C_D\,\tilde{v}}{(\zeta + h)}\,(u^2 + v^2)^{\frac{1}{2}} \tag{24}$$

where,

$$F(\eta) = \frac{\partial \xi}{\partial \eta} = 1/\{1 + \epsilon/(\xi + \xi_0)\} \tag{25}$$

Eqns. (22)-(24) form the basic set for the numerical solution process.

4. Numerical solution procedure

We write discrete coordinate points in the η-y plane as :

$$\eta = \eta_j = (j - 1)\,\Delta\eta,\ j = 1, 2, \ldots, m;\quad \Delta\eta = \eta_m/(m - 1) \tag{26}$$

where η_m is determined from (21) with $\xi = 1$,

$$\eta_m = 1 + \epsilon \ln(1 + 1/\xi_0) \tag{27}$$

We also write

$$y = y_j = (j - 1)\,\Delta y,\quad j = 1, 2, \ldots, n;\quad \Delta y = L/(n - 1) \tag{28}$$

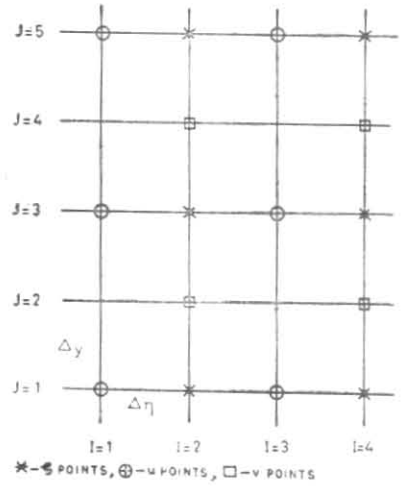

Fig. 3. Grid-point arrangement

A sequence of time-instants is defined by

$$t = t_p = p\,\Delta t, \quad p = 0, 1, \ldots \ldots \tag{29}$$

The finite-difference grid selected for the numerical solution of (22)-(24) is completely analogous to that used by Johns *et al.* (1981, 1982, 1983 a). In the η-y plane, we use a staggered grid in which there are three distinct types of computational points. With i even and j odd, the point is a ζ-point at which ζ is computed. If i is odd and j is odd the point is a u-point at which both u and U are computed. If i is even and j is even, the point is a v-point at which v is computed. Along $\eta=0$ we, therefore, have only u-points and at each of these we have $U=0$ identically. We choose m to be even so that $\eta=1$ consists of both ζ-points and v-points. We also choose n to be odd thus ensuring that there are only ζ-points and u-points along $y=0$ and $y=L$. This arrangement of grid points is shown in Fig. 3. The factor $F(\eta)$ is evaluated at each of the discrete η-points given by (26). In order to do this, relation (21) is used to determine the value of ξ at each of the discrete η-points by applying a Newton-Raphson iterative procedure. The corresponding discrete values of $F(\eta)$ are derived from (25).

Any variable χ, at a grid point (i, j) may be represented by

$$\chi(\eta_i, y_j, t_p) = \chi^p{}_{ij} \tag{30}$$

In order to describe the finite-difference equations, we define averaging operators by

$$\begin{aligned} \overline{\chi}^{\eta} &= \tfrac{1}{2}\left[\chi^p{}_{i+1,j} + \chi^p{}_{i-1,j}\right], \\ \overline{\chi}^{y} &= \tfrac{1}{2}\left[\chi^p{}_{i,j+1} + \chi^p{}_{i,j-1}\right] \\ \overline{\chi}^{\eta y} &= \overline{\overline{\chi}^{\eta}}^{y} \end{aligned} \tag{31}$$

Difference operations are defined by

$$\begin{aligned} \Delta_t \chi &= \left\{ \chi^{p+1}_{ij} - \chi^{p}_{ij} \right\} / \Delta t\,, \\ \delta_\eta \chi &= \left\{ \chi^{p}_{i+1,j} - \chi^{p}_{i-1,j} \right\} / (2\,\Delta\,\eta) \\ \delta_y \chi &= \left\{ \chi^{p}_{i,j+1} - \chi^{p}_{i,j-1} \right\} / (2\,\Delta\,y) \end{aligned} \tag{32}$$

and a shift operator is defined by

$$E_t \chi = \chi^{p+1}_{ij} \tag{33}$$

The equation of continuity, (22) is then discretised according to

$$\Delta_t(b\,\zeta) + \delta_\eta\left[b\,(\bar{\zeta}^{\eta} + h)\,U\right] + \delta_y\,\bar{v}^{y} = 0 \tag{34}$$

Eqn. (34) yields an updating procedure to compute the elevation at all the interior ζ-points and is consistent with the mass conservation in the system. The elevations at $j=1$ and $i=2, 4, \ldots, m-2$ is determined by Eqn. (10), in practice, this is applied at $j=2$ and is replaced by

$$\frac{1}{2}\left(\frac{g}{h_{i2}}\right)^{\frac{1}{2}}\left(\zeta^{p+1}_{i1} + \zeta^{p+1}_{i3}\right) + v^{p}_{i2} = 0 \tag{35}$$

thus leading to an updating procedure for the elevation on the southern open-sea boundary in the form of

$$\zeta^{p+1}_{i1} = -\zeta^{p+1}_{i3} - 2\left(\frac{h_{i2}}{g}\right)^{\frac{1}{2}} v^{p}_{i2} \tag{36}$$

Similarly, the elevations at $j=n$ and $i=2, 4, \ldots, m-2$ is determined from (11) which takes the form

$$\zeta^{p+1}_{in} = -\zeta^{p+1}_{i,n-2} + 2\left(\frac{h_{i,n-1}}{g}\right)^{\frac{1}{2}} v^{p}_{i,n-1} \tag{37}$$

The elevations along the eastern open-sea boundary $\eta=1$ is determined from (20) which yields

$$\zeta^{p+1}_{mj} = -\zeta^{p+1}_{m-2,j} + 2\left(\frac{h_{m-1,j}}{g}\right)^{\frac{1}{2}} b_j\,U^{p}_{m-1,j} \tag{38}$$

Eqn. (38) yields updated elevations for $i=m$.

Elevations along the coast at $i=1$ are not carried in our computational scheme. They are, therefore, determined by linear extrapolation from the adjacent ζ-points by using

$$\zeta^{p+1}_{1j} = \frac{1}{2}\left(3\,\zeta^{p+1}_{2j} - \zeta^{p+1}_{4j}\right) \tag{39}$$

Eqn. (23) is discretised as follows :

$$\begin{aligned} \Delta_t\,\bar{U} + \frac{1}{F}\,\delta_\eta\left[\overline{U}^{\eta}\,\bar{u}^{\eta}\right] + \delta_y\left[\overline{v}^{\eta}\,\bar{U}^{y}\right] - f\,\bar{V}^{\eta y} \\ = -\frac{g}{F}\,E_t\left[(\bar{\zeta}^{\eta} + h)\,\delta_\eta\,\zeta\right] + \frac{b\,\tau_x{}^{\zeta}}{\rho} - \\ - C_D\,\frac{\left[u^2 + (\bar{v}^{\eta y})^2\right]^{\frac{1}{2}}}{E_t\,(\bar{\zeta}^{\eta} + h)}\,E_t(\bar{U}) \end{aligned} \tag{40}$$

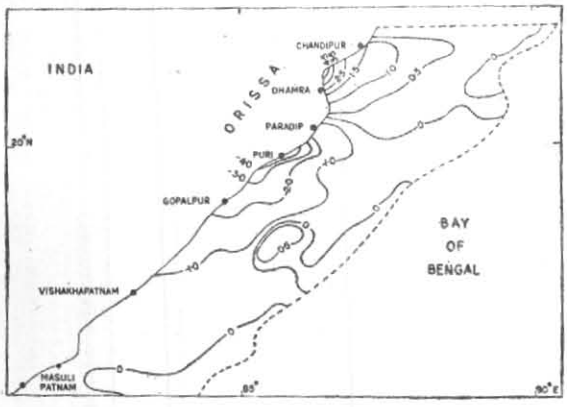

Fig. 4. Contours (in metres) of equal sea-surface elevation at 2200 IST on 3 June

This equation is used to update u at the u-points. Updated values of u may then be obtained by applying (18) as

$$E_t(u) = \frac{E_t(\bar{v})}{b_j E_t[(\bar{\zeta}^{\eta} + h)]} \tag{41}$$

Eqn. (40) is applied for $i=3, 5, \ldots, m-1$ and $j=3, 5, \ldots, n-2$. With the help of (19), the boundary value of U at $i=1$ [referenced by the averaging operator in (40)] is identically zero. When applied at $i=m-1$, the averaging operator in (40) references a value of U outside the analysis area and, to overcome this difficulty, an appropriate one-sided extrapolation of δ_η is used. Similarly, when (40) is applied at $j=3$ and $j=n-2$, the averaging operator references values of u at $j=1$ and $j=n$ and, at these positions, we also use a one-sided definition of δ_y. In this way, values of u (or u) may be updated at all the interior u-points.

A similar discretisation scheme is applied to Eqn. (24) whose finite difference form may be written as

$$\Delta_t \bar{v} + \frac{1}{F}\,\delta_\eta\,(\bar{U}^y\,\bar{\bar{v}}^{\eta}) + \delta_y\,(\bar{v}^y\,\bar{\bar{v}}^{y}) + E_t\,(f\,\bar{\bar{u}}^{\eta y})$$

$$= -gE_t\Big[b\,(\bar{\zeta}^y + h)\,\delta_y\,\zeta - \left(\frac{\partial b_1}{\partial y} + \xi\,\frac{\partial b}{\partial y}\right)\frac{(\bar{\zeta}^y + h)}{F}$$

$$\delta_\eta\,\bar{\zeta}^{\eta y}\Big] + \frac{b\,\tau_y^{\zeta}}{\rho} - \frac{C_D\,[(\bar{u}^{\eta y})^2 + v^2]^{\frac{1}{2}}}{E_t\,(\bar{\zeta}^y + h)}\,E_t\,(\bar{v}) \tag{42}$$

This equation is used to update v at the v-points. Updated values of v may then be obtained by applying (18) as

$$E_t(v) = \frac{E_t(\bar{\bar{v}})}{E_t\,[(\bar{\zeta}^y + h)]} \tag{43}$$

Eqn. (42) is applied for $i=2, 4, \ldots, m-2$ and $j=2, 4\ldots, n-1$. One sided definitions of δ_y are used when $j=2$ and $j=n-1$.

Once u and v are updated, U may also be updated by applying (17). The discretised form of this may be written as

$$U = \frac{1}{b}\left[u - \left(\frac{\partial b_1}{\partial y} + \xi\,\frac{\partial b}{\partial y}\right)\bar{v}^{\eta y}\right] \tag{44}$$

5. Stability

The stability characteristics of this computational scheme have been discussed by Johns *et al.* (1981). Infact, the computational stability is ensured by just restricting the time increment Δt governed by the CFL (Courant-Friedrich-Lewy) criterion, *i.e.*,

$$(2\,gh_{max})^{\frac{1}{2}}\,\frac{\Delta t}{\Delta x} \leqslant 1 \tag{45}$$

Taking into account the maximum depth of water h_{max} encountered within the model, a permissible value of Δt may be determined.

6. Numerical experiments

Numerical experiments are performed using the analysis area shown in Fig. 2. On average, the width of the coastal zone is about 300 km. An idealized cyclone moves along the indicated northwesterly track for about 11 hours before landfall at the north Orissa coast. Thus our experiment allows the complete recording of the surge generating capacity of the cyclone after its intensification into a severe cyclonic storm (1030 IST on 3 June 1982).

Dube *et al.* (1981) have studied the effect of different pressure and wind profiles on storm surges. However, in the absence of adequate observations, in the presen study the wind field is simulated by applying following empirically-based formula suggested by Jelesnianski (1965)

$$V = \left\{\begin{array}{ll} V_0\,(r/R)^{3/2} & \text{for } r \leqslant R \\ V_0\,(R/r)^{1/2} & \text{for } r > R \end{array}\right\} \tag{46}$$

where, V_0 is the maximum sustained wind, R the radius of maximum wind and r is the distance from the centre of the cyclone. Using reports from the India Meteorological Department, we take $V_0=50$ m s^{-1} and $R=40$ km.

In this study, we have taken $m=10$, $n=49$, $\epsilon=0.04$, $\xi_0=0.001$. Thus, $\eta_m \simeq 1.27$ and $\Delta\eta \simeq 0.14$.

It may be seen that with the above selection of parameters, the first off-shore grid-point at which the elevation is computed is, on average, about 7 km from the coastline and $\Delta y \simeq 36.5$ km.

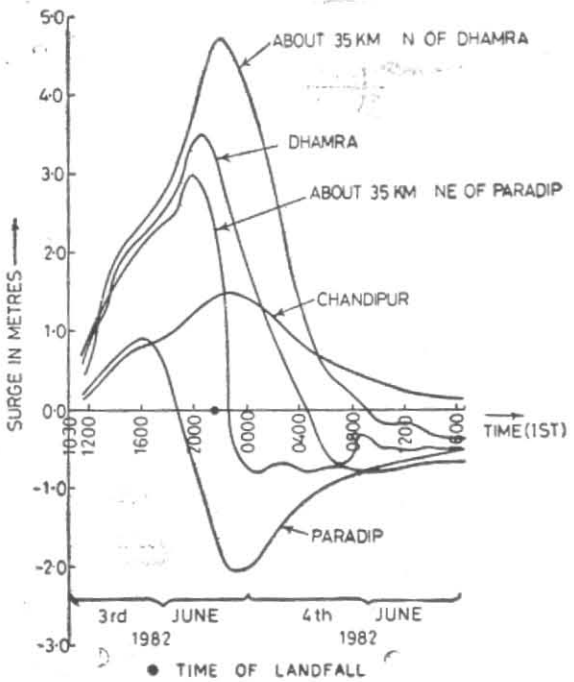

Fig. 5. Time variation of the predicted sea-surface elevation at coastal stations. The symbol ● on the time-scale indicates the time of landfall

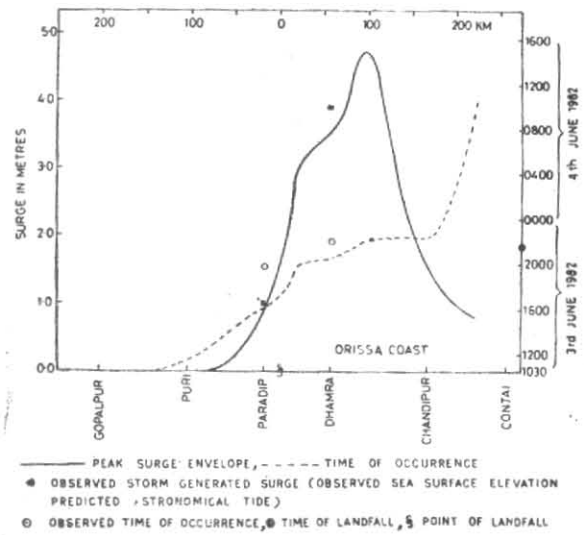

Fig. 6. Maximum sea-surface elevation and time of occurrence along north Orissa coast

In our numerical experiments, we prescribed an initial state of rest and integrated the governing equations ahead in time upto a total of 30 hours. A time-step of 3 min. was found to be consistent with computational stability. We also considered the sea surface response during the 19 hours after landfall when the system starts to enter the resurgence phase.

7. Results and discussions

In Fig. 4, contours of equal sea-surface elevation are given for coastal regions of Orissa and north Andhra Pradesh. This spatial distribution of surge correspond to about 30 min. after the landfall, that is, at 2200 IST. It may be seen from the figure that a positive surge of more than 4.5 m occurs to the right of the track (north Orissa coast), while a strong negative surge (in excess of 4 m) develops to the left of the storm (south Orissa coast). This is consistent with the local evidence of surge all along the north Orissa coast, while there was no trace of any surge to the south of Paradip. These results also confirm the earlier findings of Dube *et al.* (1982) that along the Orissa coast, which does not have significant curvature, the peak surge occurs always to the right of the landfall.

Fig. 5 depicts the time variation of storm surge at five points along the north Orissa coast. All the three stages of the surge-forerunner, the main surge, and resurgence phase may clearly be seen from the temporal variation of the coastal surface elevations. The maximum surge height of 4.8 m is predicted at a place about 35 km north of Dhamra harbour. The peak occurred at 2200 IST on the night of 3 June. This main surge remains for a very short period (less than 30 min.) and is followed by the resurgence phase. During resurgence the sea-surface elevation falls rapidly from its maximum value and becomes negative after the next 10 hours period and a sea-surface depression of about 35 cm is predicted at 1630 IST on 4 June.

The predicted time history of surge at Paradip indicate a maximum sea-surface elevation of 1 m in the afternoon of 3 June at about 1600 IST. This main surge persists for about one hour before falling rapidly and becoming negative at 1900 IST. At Paradip, a maximum sea-surface depression of about 2 m is predicted at 2300 IST (3 June) with a subsequent increase in the water height leading to a depression of about 50 cm in the afternoon of 4 June.

About 35 km to the northeast of Paradip (20 km to the NE of landfall), the predicted surge height is about 3 m which occurs at 2000 IST on 3 June. Here again the main surge is very short-lived (less than 30 min.) and the surge becomes negative within two

and half hours of the occurrence of its peak value. A sea-surface depression of 80 cm is predicted at 0030 IST on 4 June.

At Dhamra harbour, the sea-surface elevation rises gradually to attain its peak value of 3.5 m at 2030 hours IST on 3 June. This high sea-surface elevation is again short-lived and it falls rapidly to become negative in the early morning of 4 June. A negative surge of about 67 cm is predicted at 0700 IST after which the elevation changes in the form of a damped free oscillation.

In the extreme northeast of Orissa at Chandipur, the maximum predicted surge elevation of about 1.5 m occurs at 2230 IST on 3 June. The main surge continues for a period of about 2 hours after which it falls gradually during the resurgence phase and becomes 10 cm after the 30 hours of integration.

It is interesting to note from Fig. 5 that a positive surge response is predicted along the entire coast of north Orissa, where heavy inland flooding with high surge was reported to occur during the night of 3 June.

In Fig. 6 we give the distribution of the predicted maximum sea-surface elevation (peak surge envelope), observed surge and its time of occurrence along the north Orissa coast. This provides an idea of the coastal stretch upto which the significant surge may be expected. Along this portion of the Indian coast there are two tide gauge stations. The one at Paradip port is an automatic tide gauge which provides continuous record of precise tidal observations while at Dhamra port hourly tidal observations are made with the help of a graduated pole. The observation at these tidal stations indicate the elevation due to the simultaneous presence of both surge and tide. If we assume that the total sea-surface elevation is the result of purely linear superposition of surge and tide, the contribution due to the storm generated surge may be obtained by subtracting the predicted values of astronomical tides (available in the *Tide Table*) from the actually observed sea-surface elevations.

It may be seen from the figure that the maximum surge height of 4.8 m is predicted at a place which is about 90 km to the right of landfall point. The time of occurrence of this peak surge coincides with the time at which high sea-surface elevations (surge and tide) of 6-7 m were reported from the region.

A maximum surge of about 3.5 m is predicted at Dhamra port (about 55 km to the right of landfall) at 2030 IST on 3 June. A peak elevation of 6.7 m was observed at this tidal station on the night of 3 June at 2200 IST while according to tide table the predicted astronomical tide was 2.8 m at about the same time. Thus the observed sea-surface elevation was in excess by 3.9 m over the usual high tide. Hence it may be seen that our predicted surge (3.5 m) and the observed maximum surge (3.9 m) at Dhamra are in good agreement, although the model appears to produce the peak elevation about one and half hours in advance of the observed time. It may be noted here that our model predicts the surge height at the coastal boundary from where the flood wave would presumably take an additional period of time to reach the Dhamra port tidal station which is situated at the mouth of *Baitarini* river about 15 km from the sea-shore.

At Paradip, which is about 17 km to the left of the landfall point the maximum predicted surge elevation of about 1 m occurs at 1615 IST on 3 June. This is in good agreement with the observed surge of 1 m, which is obtained by subtracting the predicted tide of 2.2 m (tide table value) from the actually observed sea-surface elevation of 3.2 m. It may again, however, be noted that the model predicts the peak surge about 3 hours before the recorded time of high sea-surface elevation at Paradip. We may like to give the same reasoning to this phase discrepancy between the predicted and observed surge, as given earlier in the case of surge at Dhamra port, because the tide recorder is not situated in the open sea.

8. Concluding remarks

A coastal zone numerical model has been used to simulate the surge generated by June 1982 Orissa cyclone. On the basis of the above results following general conclusions may be made :

(*i*) The predicted maximum surge elevation and its time of occurrence along the north Orissa coast compares well with the actual observations.

(*ii*) Thirty-hour of simulation of the surge takes about 5 minutes of computer time on an ICL 2960 computer for a grid of 10 by 49 points. The model can be used for simulating the surge generated by the cyclone of any speed or intensity. It may also be used for estimating the surge on real time basis.

Acknowledgements

The authors are grateful to Mr. K. S. Chandrasekeran, Special Relief Commissioner, Govt. of Orissa, for providing the necessary facilities in carrying out

post-storm survey in the coastal districts of north Orissa. We would like to express our thanks to Paradip Port Trust authorities and the Conservator of Dhamra Harbour for providing the valuable data on observed sea-surface elevations which proved very useful in validating the results of the study. Thanks are also due to Prof. M. P. Singh, Head, Centre for Atmospheric Sciences, Indian Institute of Technology, New Delhi for his continued interest in the work.

References

Das, P.K., 1972, Prediction model for storm surges in the Bay of Bengal, *Nature*, **239**, 211-213.

Das, P.K., 1981, Storm surges in the Bay of Bengal, *Proc. Indian Acad. Sci.* (*Engg. Sci.*), **4**, 269-276.

Das, P.K., Sinha, M.C. and Balasubramanyam, V., 1974, Storm surges in the Bay of Bengal, *Quart. J. R. met. Soc.*, **100**, 437-449.

Dube, S.K., Sinha, P.C. and Rao, A.D., 1981, The response of different wind-stress forcings on the surge along the east coast of India, *Mausam*, **32**, 315-320.

Dube, S.K., Sinha, P.C. and Rao, A.D., 1982, The effect of coastal geometry on the location of peak surge, *Mausam*, **33**, 445-450.

Jelesnianski, C.P., 1965, A numerical calculation of storm tides induced by a tropical storm impinging on a continental shelf, *Mon. Weath. Rev.*, **93**, 343-358.

Johns, B., 1981, Numerical simulation of storm surges in the Bay of Bengal, *Proc. on Monsoon Dynamics*, Cambridge University Press, 689-705.

Johns, B. and Ali, A., 1980, The numerical modelling of storm surges in the Bay of Bengal, *Quart. J. R. met. Soc.*, **106**, 1-18.

Johns, B., Dube, S.K., Mohanty, U. C. and Sinha, P. C., 1981, Numerical simulation of the surge generated by the 1977 Andhra cyclone, *Quart. J. R. met. Soc.*, **107**, 919-934.

Johns, B., Dube, S.K., Sinha, P.C., Mohanty, U.C. and Rao, A.D., 1982, The simulation of continuously deforming lateral boundary in problems involving the shallow water equations, *Computers and Fluids*, **10**, 2, pp. 105-116.

Johns, B., Sinha, P.C., Dube, S.K., Mohanty, U.C. and Rao, A.D., 1983(a), On the effect of bathymetry in numerical storm surge simulation experiments, *computers and Fluids*, **11**, 3, pp. 161-174.

Johns, B., Sinha, P.C., Dube, S.K., Mohanty, U.C. and Rao, A.D., 1983(b), Simulation of storm surges using a three-dimensional numerical model : An application to the 1977 Andhra cyclone, *Quart. J. R. met. Soc.*, **109**, 211-224.